Journal of Alloys and Compounds 968 (2023) 171928

Contents lists available at ScienceDirect

Journal of Alloys and Compounds

journal homepage: www.elsevier.com/locate/jalcom

Using direct high-pressure torsion synthesis to produce aluminium matrix nanocomposites reinforced with carbon nanotubes

Maria Emerla [a], Piotr Bazarnik [a,*], Yi Huang [b,c], Małgorzata Lewandowska [a], Terence G. Langdon [b]

[a] Warsaw University of Technology, Faculty of Materials Science and Engineering, Woloska 141, 02-507 Warsaw, Poland
[b] Materials Research Group, Department of Mechanical Engineering, University of Southampton, Southampton SO17 1BJ, United Kingdom
[c] Department of Design and Engineering, Faculty of Science and Technology, Bournemouth University, Poole, Dorset BH12 5BB, United Kingdom

ARTICLE INFO

Keywords:
Aluminium
Carbon nanotubes
High-pressure torsion
Nanocomposites
Thermal stability

ABSTRACT

Aluminium matrix nanocomposites reinforced with carbon nanotubes were fabricated in a new way by direct synthesis using high-pressure torsion (HPT). Aluminium of 99.99 % and 99.5 % purities were used as matrix materials with carbon nanotubes in amounts of 0.5 and 1 wt% as reinforcement. The HPT processing led to extensive grain size refinement which was significantly higher than for pure metals and to a relatively uniform distribution of the fillers. The grain size of the matrix was smaller for Al99.5 compared to Al99.99 while the particle spatial distribution was more homogenous for the Al99.99 matrix. This was attributed to a lower hardness and higher plasticity of Al 99.99 alloy. The addition of carbon nanotubes also improved the thermal stability of the ultrafine-grained structure, especially if homogenously distributed as for the Al99.99 matrix nanocomposites.

1. Introduction

The continuous development of applied technologies in the automotive, aerospace and electronics industries, as well as contemporary efforts to protect the natural environment by reducing emissions of exhaust and greenhouse gases, have contributed to numerous studies seeking effective methods to significantly improve the mechanical properties of metal alloys and composites with favourable strength-to-density ratios [1–4]. One of the developmental paths leading to the improvement of strength, hardness and wear resistance of such metallic materials is a significant refinement of their grain structure where this can be achieved by, among others, the use of processing through the application of severe plastic deformation (SPD) [5–9]. Among a number of SPD methods, High-Pressure Torsion (HPT) is considered the most effective in terms of grain size refinement due to the large plastic strains introduced to the material [5,7].

Several studies have demonstrated that HPT processing leads to a significant increase in hardness and tensile strength in many engineering materials [7,10,11] due to the production of severe grain refinement to the sub-micrometric and nanometric sizes. Nevertheless, the ability of each material to achieve grain refinement is limited so that ultimately the grain size saturates at a certain level [11–17]. Moreover, the purity level of metals also has a significant impact on the final structural refinement. For example, high purity Al (99.9999 %) undergoes HPT-induced softening due to grain growth during the processing whereas a commercial purity Al (99.5 %) exhibits a strain hardening during processing [18]. This softening effect is caused by the high mobility of dislocations and the role of grain boundaries as dislocations sinks which are significantly influenced by the presence of impurity atoms [19].

Additionally, ultra-fine grained (UFG) and nanocrystalline (NC) metals are inherently thermally unstable so that annealing, even at low temperatures, leads to recrystallisation and grain growth of the microstructure and this is deleterious to the material properties [20–22].

In order to improve the thermal stability of these types of materials and stabilise the grain sizes at elevated temperature, some limited attempts have been made to create metal matrix nanocomposites reinforced with various particles such as Al_2O_3, multi-walled boron nitride nanotubes (BNNTs),or carbon nanotubes (CNTs) [23–25]. Nano-particles uniformly distributed within the metallic matrix constitute a pinning effect on lattice defects, such as dislocations and grain boundaries, thereby stabilising the UFG microstructure and expanding

* Corresponding author.
E-mail address: piotr.bazarnik@pw.edu.pl (P. Bazarnik).

https://doi.org/10.1016/j.jallcom.2023.171928
Received 6 June 2023; Received in revised form 8 August 2023; Accepted 27 August 2023
Available online 28 August 2023

the temperature window for their potential technological applications.

There are only a few reports describing Al-CNTs nanocomposites subjected to HPT processing [26–28]. Furthermore, a review of these reports shows that all of the nanocomposites were fabricated in multi-stage procedures in which the HPT processing was always preceded by powder metallurgy synthesis such as ball milling of the powders followed by conventional sintering [29,30], hot pressing [31,32], spark plasma sintering [33,34] or hot extrusion[34]. The aim of the present work was to remove this time-consuming pre-treatment step and to produce an Al-CNTs nanocomposite using HPT as a direct mixing method by forming a sandwich of CNTs between two pure Al plates with different purity levels ranging from 99.5 % to 99.99 %. This objective was inspired by recent publications describing the fabrication of metal composites and metastable alloys by directly packing alternating disks of different metals for the HPT processing [35–37]. To date, only some limited publications describe any thermal stability studies of these types of materials [28,38]. Accordingly, the present report provides a detailed description of the mechanical properties, thermal stability and microstructural characteristics of Al-CNTs nanocomposites produced by this new procedure of direct HPT processing.

2. Experimental material and procedures

High and commercial purity aluminium, Al99.99 and Al99.5 %, respectively, in the form of rods of 10 mm diameter were used as a matrix while multi-walled CNTs with tube diameters of 2–5 nm were used as the reinforcement. The Al-CNTs nanocomposites with 0.5 and 1 wt% of CNTs were produced by direct HPT synthesis. Specifically, a stack of two aluminium disks with diameters of 10 mm and thicknesses of 0.4 mm, with CNTs placed between them, were subjected to HPT processing under a pressure of 1 GPa through a total number of 50 turns. Fig. 1 schematically illustrates the process for the direct synthesis of nanocomposites by HPT. In addition, 1 mm thick aluminium disks of both purities were HPT processed under the same pressure for up to 10 revolutions and these disks served as reference samples.

To investigate the thermal stability, the HPT-processed Al-CNTs nanocomposites and HPT-processed aluminium disks were annealed for 1 h at temperatures of 100ºC, 150ºC, 200ºC, 250ºC, 300ºC, 350ºC or 400ºC. The annealing was conducted in a protective argon atmosphere and the accuracy of maintaining the set temperature was ± 5°C.

Initial observations of cross-sections of the disk samples were made using a Zeiss Axio Observer optical microscope (OM). These observations were carried out on disk samples after 10, 20 and 50 revolutions in order to determine the level of mixing of the CNTs with the matrix material and also to evaluate the quality of bonding along the diameter of the disk. Images of the entire cross-sections of each sample were obtained by assembling a series of photographs using the Adobe Photoshop graphics program. The samples for OM observations were prepared by cutting the disks along their diameters using a circular saw, encapsulating the samples in resin, grinding the samples on sandpaper and then polishing the samples using a 1 μm diamond suspension.

Advanced structural observations of the fabricated nanocomposites

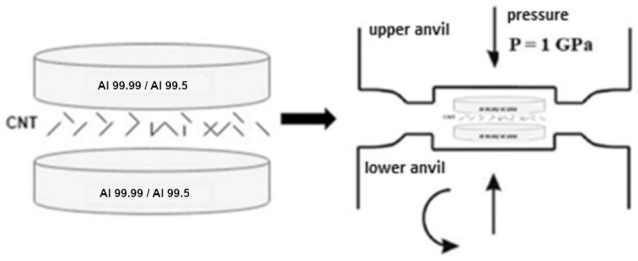

Fig. 1. Schematic of sandwich carbon nanotubes between two aluminium disks for HPT processing.

before and after annealing were collected using a scanning electron microscope (SEM) Hitachi Su8000 operating in back-scattered electron (BSE) mode. Observations were carried out on cross-sectional planes approximately 1 mm from the edges of the disks. Samples for SEM investigations were prepared using an Hitachi IM4000 ion milling system. This procedure gives high-quality surfaces for observation due to the ion beam polishing which eliminates any deformation, stresses and/or the formation of oxide layers. The surface quality after the ion milling process permitted the structure to be observed in so-called channel contrast in the SEM.

The average grain sizes together with the standard deviations, were measured based on SEM/BSE image analysis. NIS-Elements BR 3.2 software was used to analyse the grain size and its variability and GIMP 2 software was used to prepare the SEM images for analysis. Detailed microstructural observations were performed using a scanning-transmission electron microscope (STEM) Hitachi HD-2700 operating at an accelerating voltage of 200 kV. Samples for the STEM observations were prepared using a focused ion beam facility (FIB) Hitachi NB5000.

A Falcon 503 hardness tester was employed to determine the Vickers hardness of the samples before and after annealing using a 200 g load for each measurement. Hardness values were recorded on cross-sections of the specimens with a 0.3 mm distance between each indentation. Hardness measurements for the annealed specimens were taken approximately 1 mm from the edge of the disk with a 0.2 mm spacing between indentations. Prior to these hardness measurements, the specimens were encapsulated in resin and the cross-sectional surfaces of the disks were mechanically ground and then polished using a 3 μm anhydrous diamond suspension in order to remove any oxides.

3. Experimental results

3.1. Microstructure of Al-CNTs nanocomposites

Fig. 2 shows a series of OM images of the cross-sectional areas of Al99.5 and Al99.99 with 0.5 % and 1 % of CNTs nanocomposites after HPT processing through 10, 20 and 50 turns. These images provide clear evidence for the gradual evolution towards nanocomposites. A large structural variation can be observed depending on the number of rotations. With increasing numbers of HPT turns, there is an obvious improvement in the distribution of CNTs in the aluminium matrix and thus a reduction in the number of large and visible CNTs agglomerates. Since the CNTs were applied directly between two aluminium disks, they tended to accumulate along the horizonal axis of the disk sample especially near the centre of each disk. For all nanocomposites, more dispersed CNT particles in the aluminium matrix are observed with higher numbers of turns and increasing distance from the disk centres. Inspection shows that samples of all nanocomposite types after 10 and 20 HPT rotations have visible long bands of CNTs agglomerates while in the samples after 50 rotations such bands are much less visible so that there is an improved dispersion of CNTs throughout the samples. The only exception is the Al99.5–1 % CNTs sample for which a significant proportion of CNTs agglomerates remains visible in the central regions. In addition, it is noticeable that in the nanocomposites based on Al99.99 the CNTs particles exhibit a higher tendency to be uniformly distributed in the matrix by comparison with Al99.5.

The polished surfaces of the Al-CNTs samples were further observed by SEM at higher magnifications to reveal the grain structure. The results are presented in Fig. 3 and for comparative reasons were complemented with images for pure aluminium samples of both purities processed through 10 HPT turns. These microstructures were evaluated quantitatively using a computer-aided image analyser. The grain sizes described in terms of the equivalent grain diameter (d) and the standard deviation (SD) are summarised in Table 1.

The average grain sizes in pure Al99.5 and Al99.99 after 10 HPT turns were 670 and 830 nm (Fig. 3), respectively, and this is consistent with results reported for materials processed using conventional SPD

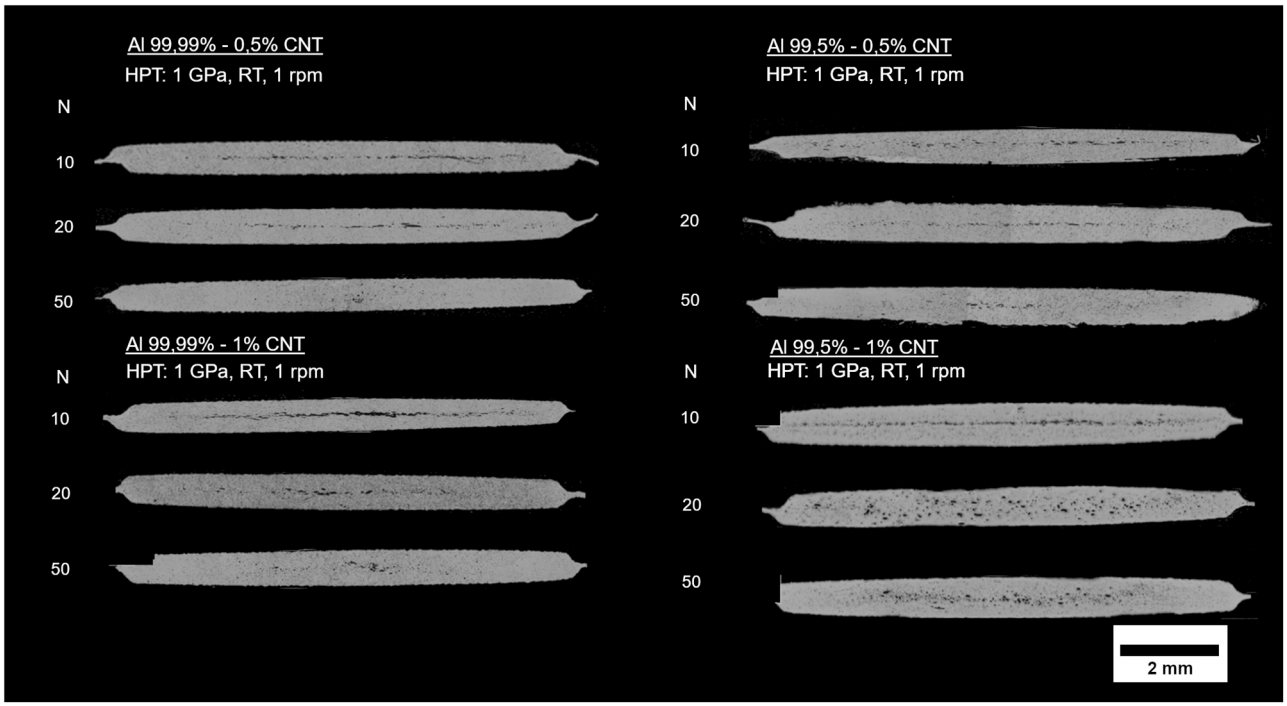

Fig. 2. Light microscopy views of cross-sections of HPT-processed composites.

methods [18,39,40]. The addition of CNTs led to more intense grain refinement in the metal matrix in both nanocomposites, as is evident from Fig. 3 and Table 1. After 10 HPT revolutions, the grain size was reduced to ~800 nm in the Al99.99 matrix nanocomposites and below ~450 nm in the Al99.5 matrix nanocomposites. A further decrease in grain size was observed with increasing numbers of turns such that, after 50 turns, the average grain sizes of the aluminium matrices for all nanocomposites was below ~250 nm (Table 1). The matrix structure in all nanocomposites consisted of equiaxed grains and the grain size scatter was typical for fairly homogenous materials. The smallest grain size in the aluminium matrix of ~190 nm was obtained for the Al99.5 matrix nanocomposite containing 1 % of CNTs.

It is important to note that, although the structure of the matrix is reasonably homogeneous, the distribution of CNTs is not homogeneous. Fig. 4a and b show SEM images of the edge region for Al99.99 containing 0.5 % of CNT after 10 and 50 HPT turns, respectively. It is apparent that the CNTs are mostly distributed in the form of micro-sized agglomerates and in the form of chains along grain boundaries after 10 revolutions whereas after 50 revolutions many of these larger agglomerates are fragmented to sizes of ~20–200 nm and they become uniformly distributed in the aluminium matrix. However, the size and the density of the CNTs agglomerates strongly depends on the purity of the aluminium matrix. Fig. 4c and d were taken at the same magnification and they illustrate the microstructures after 50 HPT revolutions for Al99.99 – 0.5 % CNTs and Al99.5–0.5 % CNTs, respectively. These images show that the agglomerates are smaller and their density is lower in the purer metal and this tendency was observed in all samples.

In order to better describe the distribution of CNTs in the matrix, a series of SEM images was analysed in terms of the average size and the surface fraction of CNTs agglomerates that were larger than ~150 nm and the results are summarised in Table 2. In general, for small numbers of revolutions it is apparent that mostly large agglomerates dominate the structures with their size and surface fraction associated with the amount of CNTs used. With increasing numbers of revolutions, there is an observed decrease in both the size of the agglomerates and their surface fraction. It is also be noted that this tendency is less for the Al99.5 matrix than for the Al99.99 matrix.

Figs. 5 and 6 shows exemplary STEM images of, respectively, Al99.99 and Al99.5 samples containing 0.5 % of CNTs processed through 50 HPT revolutions. The comparative HAADF and BF images of Al99.99 (Fig. 5a, b) and Al99.5 (Fig. 6a, b) matrix nanocomposites confirmed the significant grain refinement with an average grain size of ~200 nm in both aluminium matrices and large differences in the size and distribution of CNTs agglomerates which are shown black in the HAADF contrast. The agglomerates in the Al99.5 matrix nanocomposite are larger and their number is greater than in the Al99.99 matrix nanocomposite. At the same time, only a fraction of individual CNTs are visible in the matrix of the Al99.5 nanocomposite (Fig. 6c) whereas in the Al99.99 nanocomposite there are a number of small (<100 nm) uniformly distributed agglomerates (Fig. 5b) as well as individual CNTs (Fig. 5c) within the matrix.

3.2. *Mechanical properties of Al-CNTs nanocomposites*

The microhardness of the fabricated nanocomposites were measured on the cross-sections of the disks and the results are shown in Fig. 7a and b as a function of distance from the disk centres. These plots demonstrate that HPT processing has enhanced the hardness in both types of nanocomposites and, in general, the hardness of the nanocomposites increases with increasing numbers of revolutions and concentration of CNTs. The highest values of hardness were obtained in samples containing 1 wt% of CNTs subjected to 50 HPT rotations. Thus, the hardness values increased from 25 and 50 Hv for HPT-processed Al99.99 and Al99.5 pure metallic samples to 80 and 110 Hv, respectively, at the edges of the HPT-processed nanocomposites containing 1 wt% of CNTs. Although the hardness after 50 HPT turns was higher for the Al99.5 matrix nanocomposites, the hardness distribution was more homogeneous for the Al99.99 matrices.

The hardness for the Al99.99 matrix nanocomposites rises rapidly during HPT and already after 10 turns it is almost two times higher in the edge regions than in the pure metal after HPT (Fig. 7a). It is also apparent that there is a significant impact of the CNTs content on the hardness distribution for lower numbers of turns. Nanocomposites containing 1 wt% of CNTs exhibit higher hardness than those with 0.5 %

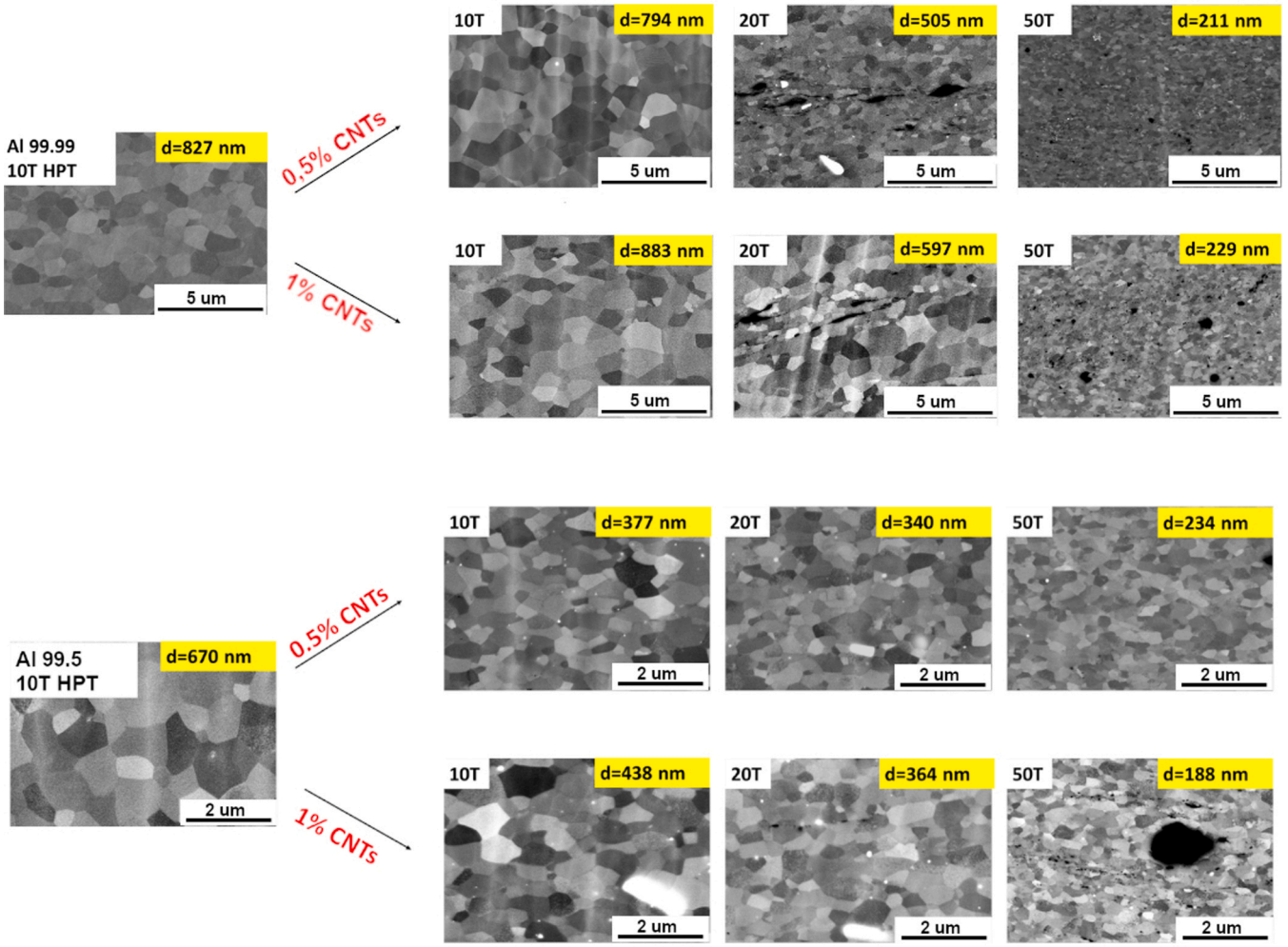

Fig. 3. Microstructure of Al 99.99 and Al 99.5 alloys after HPT processing and the microstructure of their composites containing 0.5 % and 1 % of CNTs after various numbers of HPT revolutions.

Table 1
Summary of grain sizes and standard deviations from grain sizes for individual samples.

Sample	Turns nr.	d [nm]	SD [nm]
Al 99,5 %	10	670	216
Al 99,5 % 0,5 % CNT	10	377	150
	20	340	136
	50	234	95
Al 99,5 % 1 % CNT	10	438	176
	20	364	137
	50	188	72
Al 99,99 %	10	827	352
Al 99,99 % 0,5 % CNT	10	794	377
	20	506	138
	50	211	77
Al 99,99 % 1 % CNT	10	883	417
	20	597	262
	50	229	84

which is clearly visible in the samples after 20 HPT turns for which the difference in hardness was higher than 15 Hv. Further processing up to 50 turns gave an additional hardness increase up to ~75 Hv in the edge regions with some small areas of lower hardness near the centre of the disk.

In the Al99.5 matrix nanocomposites, the results of hardness in the samples having 0.5 and 1 wt% of CNTs after 10 and 20 turns are close and only ~10 Hv higher than for pure aluminium after HPT processing and the hardness values are almost homogeneous across the disk diameters. By contrast, after 50 revolutions there is a further increase in hardness values in the edge regions such that the hardness values reach ~75 and ~100 Hv for nanocomposites containing 0.5 and 1 wt% of CNTs, respectively.

3.3. Thermal stability of Al-CNTs nanocomposites

Fig. 8 shows the average hardness measured at the disk edges for the nanocomposites after 50 HPT turns and subsequent annealing at temperatures ranging from 100 °C to 400 °C for 1 h. These results are also complemented with the hardness values for the initial materials after 10 HPT turns. The results show that UFG Al99.99 and UFG Al99.5 are thermally stable up to 150 °C and 200 °C, respectively, and these results are in agreement with earlier reports [28,41]. As can be seen, the addition of CNTs contributes to increases in the hardness for both types of nanocomposites compared to the matrix as well as to their thermal stability.

The results for the Al99.99 matrix nanocomposites indicate that the hardness remains stable until annealing at a temperature of 400 °C where there is a small drop in the hardness values (Fig. 8a). The thermal stability of the Al99.5 based nanocomposite is not as good as the Al99.99 material. Furthermore, the hardness changes more significantly and the drop strongly depends on the concentration of the CNTs. Thus, the average hardness of the Al99.5 composites is reduced after annealing at 250 °C for 0.5 wt% of CNTs by ~ 16 % and for 1 wt% of CNTs composite

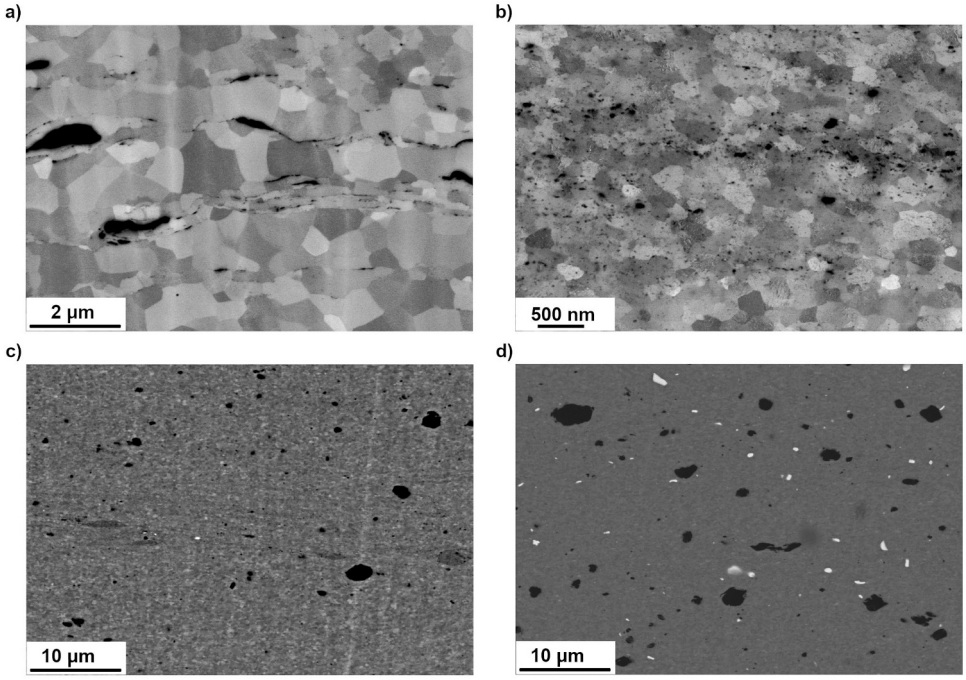

Fig. 4. SEM images of Al99.99 + 0.5 % CNTs composite after a) 10 and b) 50 HPT turns, together with comparative microstructural images taken at the same magnification for c) Al99.99 + 0.5 % CNTs and d) Al99.5 + 0.5 % CNTs, where dark regions are CNTs agglomerates.

Table 2
The average size of CNTs agglomerates and their fraction surface.

Sample		d [nm]	SD [nm]	surface fraction [%]
99.99	0.5 % CNT 10 T	590	3100	5.7
	0.5 % CNT 20 T	440	550	-
	0.5 % CNT 50 T	300	260	1.2
99.99	1 % CNT 10 T	740	4580	8.9
	1 % CNT 20 T	580	890	-
	1 % CNT 50 T	360	707	1.8
99.5	0.5 % CNT 10 T	910	8410	6.8
	0.5 % CNT 20 T	620	1550	-
	0.5 % CNT 50 T	520	950	3.4
99.5II	1 % CNT 10 T	1355	9560	9.2
	1 % CNT 20 T	750	2125	-
	1 % CNT 50 T	550	1045	4.5

after annealing at 350 °C by ~ 30 %, respectively, and a further drop of hardness is observed with annealing temperature. Nevertheless, it is interesting to note the standard deviations of the values for these results which are marked in Fig. 8b since, although the results for the nanocomposites having 0.5 % of CNTs seem to be stable up to 300 °C, at the same time they show a very large standard deviation by up to 18 Hv.

Such behaviour is explained by conducting microstructural observations. An SEM analyses of the Al99.99 matrix nanocomposites revealed their excellent thermal stability as illustrated in Fig. 9. Thus, the grain structure was stable up to a temperature of 400 °C where only slight grain growth was observed in both nanocomposites by only 10–15 % compared to the composites after HPT processing. The Al99.5 matrix nanocomposites maintained a homogeneous ultrafine-grained structure with an average grain size comparable to the material before annealing up to temperatures of 350 °C and 250 °C for the nanocomposites containing 0.5 % and 1 % of CNTs, respectively (see Figs. 10 and 11). Above these temperatures, there was an onset in the formation of a heterogeneous structure in both nanocomposites such that single large recrystallised grains, up to tens to hundreds of μm in size, surrounded by nanosized regions were observed in these structures. As the temperature increased, more regions of heterogeneous grain growth appeared in the microstructure. Moreover, it should be emphasised that in the sample

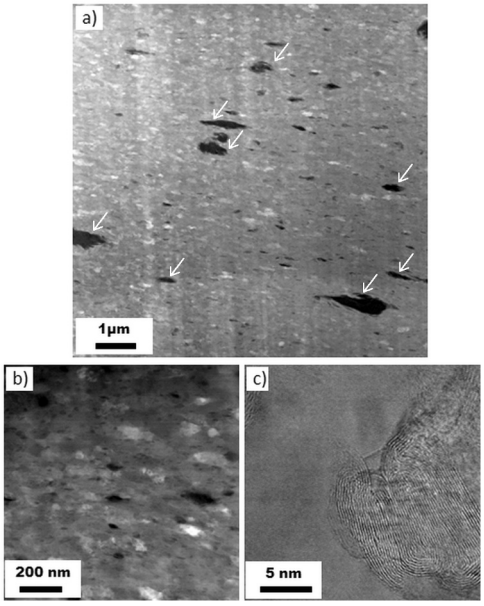

Fig. 5. STEM and HAADF a), b) images showing the microstructures of samples Al99.99 + 0.5 %CNTs processed by 50 HPT turns (with marked dark regions of CNTs biggest agglomerates), together with high resolution STEM image c) showing the interface between CNTs and the Al matrix.

containing 1 % of CNTs heterogeneous grain growth was more intense than in the sample containing 0.5 % of CNTs. After annealing at 400 °C, most of microstructure consisted of fully recrystallised large grains but there remained some places with highly refined grains although their fraction was small. Fig. 12 shows an STEM image of such a heterostructure cut from the Al99.5 sample containing 0.5 % of CNTs annealed at 350 °C. In this image there are regions with large recrystallised grains coexisting with those having UFG dimensions. In addition, there are large agglomerates (marked with arrows) of CNTs and single tubes

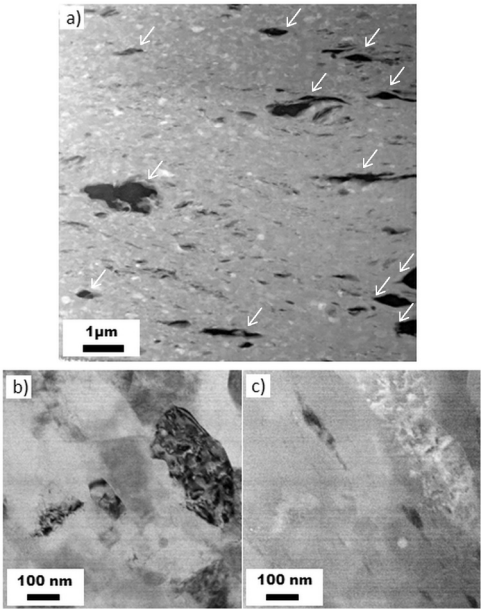

Fig. 6. STEM and HAADF images showing the microstructures of samples Al99.5 + 0.5 %CNTs processed by 50 HPT turns (with marked dark regions of CNTs biggest agglomerates), together with high resolution STEM image.

located at grain boundaries within the microstructure. At the same time it should be noted that these single CNTs are located mainly in areas with small grains.

4. Discussion

4.1. Fabrication of Al-CNTs nanocomposites via direct HPT synthesis

The results of this research demonstrate that Al-CNTs nanocomposites with fairly homogenous microstructures may be achieved by direct mixing in HPT processing. Comparing the microstructures of the processed nanocomposites with the matrix materials (Al99.99 and Al99.5) after HPT, it is shown that the addition of CNTs leads to a significantly smaller grain size in the HPT process. The effect of the addition of second phase particles on enhanced grain refinement in HPT processing was previously reported for other systems [6,30] but the present results are the first demonstration using a direct synthesis method. This phenomenon is explained by the pinning effect imposed by nanoparticles on lattice defects, such as dislocations and grain boundaries, which effectively reduces the ability of a material to exhibit recovery and recrystallisation during processing [42–44].

In these nanocomposites, the purity of the matrix material (Al99.99 and Al99.5) had a noticeable effect on the distribution of CNT particles within the matrix. For the Al99.99 matrix, which is characterised by lower hardness and thus higher ductility than Al99.5, fewer CNTs agglomerates were observed and their sizes were smaller. Numerical and experimental studies indicate that the turbulent flow of the material during the HPT deformation plays a crucial role in the fragmentation of agglomerates and the distribution of individual reinforcing phases in the matrix [45,46]. Blocking of the shear deformation in the sample undergoing HPT leads to the mixing of the material and thus an improved distribution of reinforcement phases. It is probable that the higher ductility of the Al99.99 matrix was associated with easier and faster mixing of CNTs into the matrix during HPT processing which thereby led to their more uniform distribution in the matrix. It should be noted that, besides breaking of the CNTs agglomerates during HPT processing, a fragmentation of individual CNTs also occurred. Despite this, many of them have retained their tubular structure, as shown in Fig. 5c.

It is worth noting that the improved distribution of CNTs in the Al99.99 matrix enhanced the process of grain refinement such that the grain size was ~830 nm and ~220 nm for the pure matrix and the nanocomposite, respectively, but smaller grain sizes of ~190 nm were achieved for the nanocomposites based on Al99.5 1 %CNT. This relationship is also reflected in the hardness measurements as the nanocomposites based on Al99.5 exhibited higher values of hardness in the edge areas of disk samples. This is in agreement with earlier studies on the effect of the degree of purity of the aluminium alloy on the fragmentation of the structure during the HPT process [18,47]. It should be emphasised that the addition of CNTs benefits in increasing the hardness of the nanocomposite after HPT but only if a high degree of dispersion of the reinforcing particles is achieved within the matrix. For Al99.99 matrix nanocomposites where a good distribution of the CNTs was observed, the hardness values increase even after 10 revolutions, whereas in the Al99.5 matrix nanocomposites a significant increase in hardness, associated with a better distribution of CNTs), was observed only at the disk sample edge area after 50 revolutions.

4.2. Tailoring of the mechanical properties in Al-CNTs nanocomposites

In general, the hardness of the fabricated nanocomposites depends on four factors: (1) the purity of the aluminium matrix [18], (2) the grain size as described by the Hall-Petch relationship [5], (3) density of dislocations and (4) the dispersion of CNTs. The Al99.99 matrix

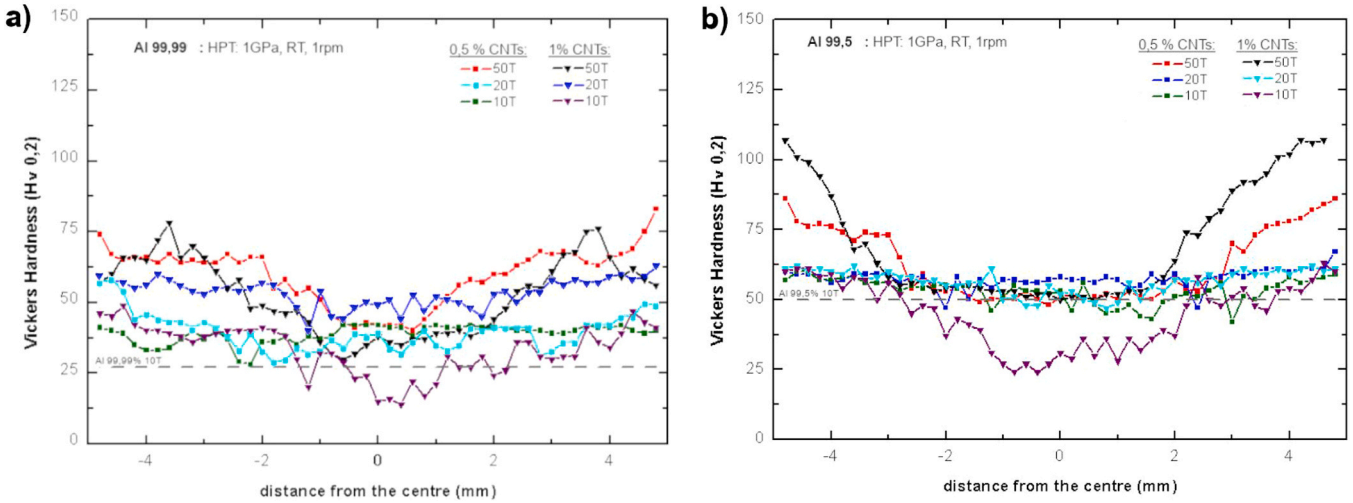

Fig. 7. Linear Hardness on the diameters of the cross-sections of samples: a) Al 99,99 composites b) Al 99,5 composites.

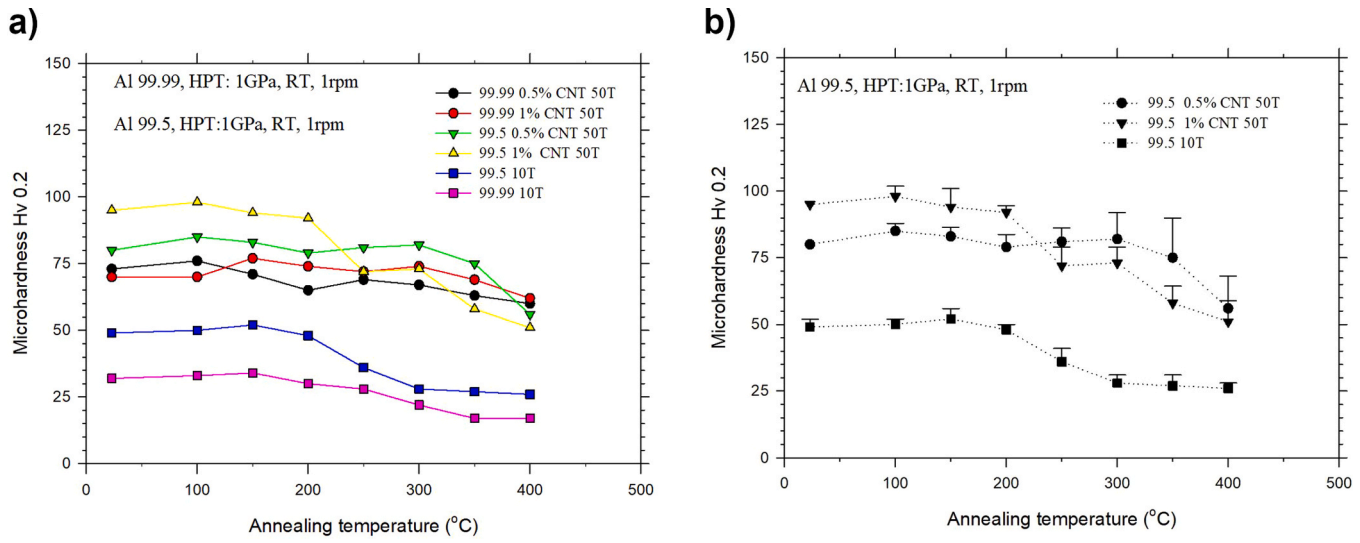

Fig. 8. The hardness of a) the Al99.99 and Al99.5 composites as a function of annealing temperature and b) hardness results for Al99.5 composites complemented with standard deviation bars.

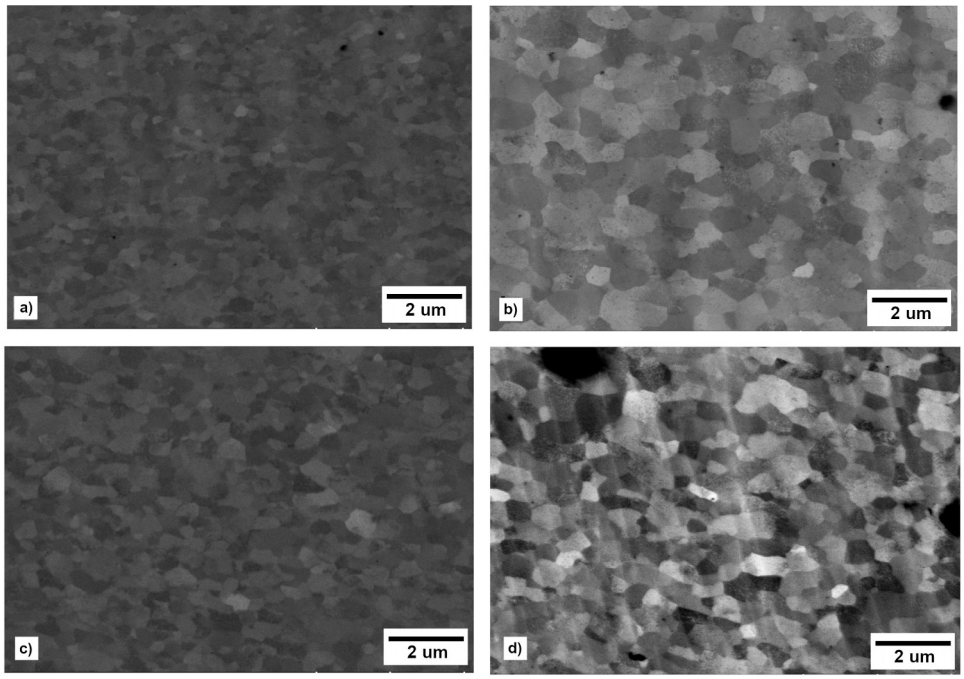

Fig. 9. Representative microstructural images of Al 99,99 0,5 % CNT composite after annealing at a) 250°C and b) 400°C; and Al 99,99 1 % CNT composite after annealing at c) 250°C and d) 400°C.

nanocomposites exhibit lower hardness when compared with the Al99.5 matrix nanocomposites mainly due to the higher purity and larger grain size of the matrix so that the better dispersion of CNTs is unable to compensate this loss. Nevertheless, the present results clearly indicate that this new approach for the production of nanocomposites using direct mixing by HPT is probably at least competitive, if not superior, to the traditional methods consisting of several stages of milling and sintering followed by HPT.

To place the results of this work in a broader perspective, Table 3 summarises the mechanical properties of the fabricated Al-CNTs nanocomposites with various Al-C alloys produced by traditional methods [10,26,27,48]. A careful review of these data provides clear confirmation that the direct processing via HPT of Al-CNTs nanocomposites presented in this work produces a material with a comparable microstructure and mechanical properties to other nanocomposites [10, 26,27,48].

It was shown in many earlier studies that the microstructural fragmentation and increase in hardness during HPT processing for many materials occur up to a certain strain and thereafter a saturation effect occurs so that at higher strains there is no additional increase in hardness or further grain size reduction [8,14,15]. The experimental points in Fig. 7 tend to be scattered but it was noted in a very early investigation of HPT that it should be possible to correlate these various points by plotting the data in the form of the values of Hv against the equivalent strain (Fig. 13) and this type of plot should also provide a direct measure of the saturation hardness [11,49]. It is apparent from Fig. 13 that the saturation effect was strongly related to the type of matrix used to produce the nanocomposites. In the nanocomposites with the Al99.99

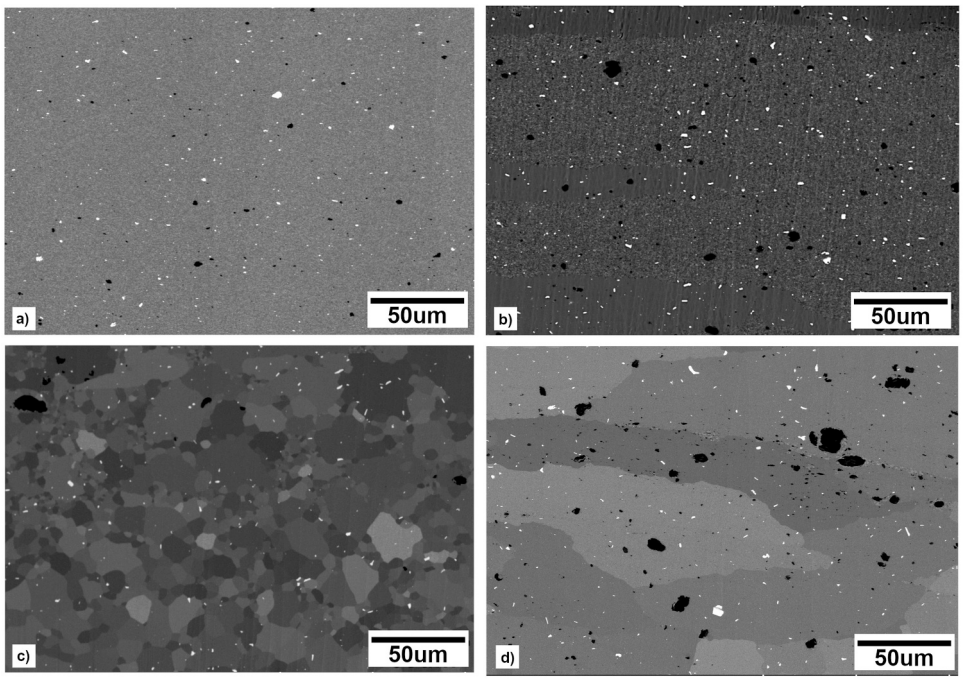

Fig. 10. Representative microstructural images of Al 99,5 0,5 % CNT after annealing at: a) 250ºC; b) 300ºC; c) 350ºC; d) 400ºC.

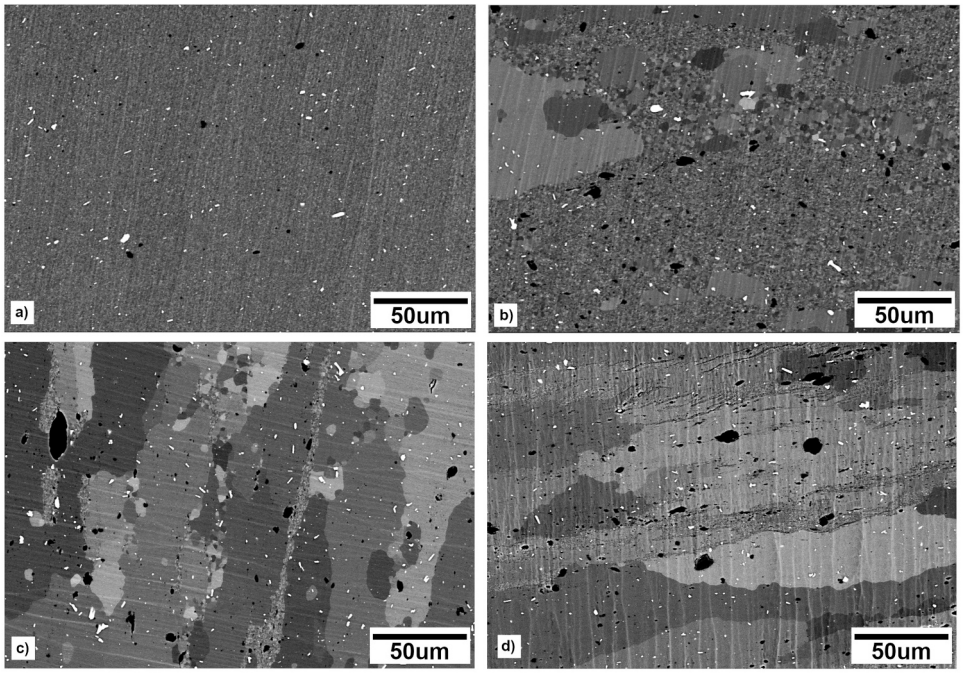

Fig. 11. Representative microstructural images of Al 99,5 1 % CNT composite after annealing at: a) 200ºC; b) 250ºC; c) 300ºC; d) 350ºC.

matrix in Fig. 13a, the increase in hardness is visible from the beginning of processing and the microhardness was not saturated until the equivalent strain exceeded ~1000. This indicates that the Al99.99 nanocomposites possess a stronger strain hardening ability than pure metal during HPT processing [5]. For the Al99.5 nanocomposites, the hardening behaviour is different as shown in Fig. 13b since the microhardness values tend to saturate in the first stage but then, after exceeding an equivalent strain of ~800, there is a strong increase in hardness which is probably associated with the dispersion of CNTs in the matrix. In materials with a good dispersion of CNTs, such as Al99.99, a significant grain refinement was observed even at 10 revolutions as in Fig. 2 whereas in the Al99.5 nanocomposites, in which a small number of revolutions such as 10 and 20 turns failed to produce a good distribution of CNTs as in Fig. 2, the hardness values saturated at a level of ~55 Hv. Thereafter, a good distribution of CNTs was achieved after exceeding a certain critical level of equivalent strain and this led to a reduction in grain size and a further increase in the microhardness values.

The present results in Fig. 3 and Table 1 show that the use of HPT processing to fabricate Al-CNTs nanocomposites leads to a pronounced microstructural refinement and an enhancement in the mechanical properties. However, such a significant increase in hardness of the nanocomposites cannot be explained only by Hall-Petch strengthening

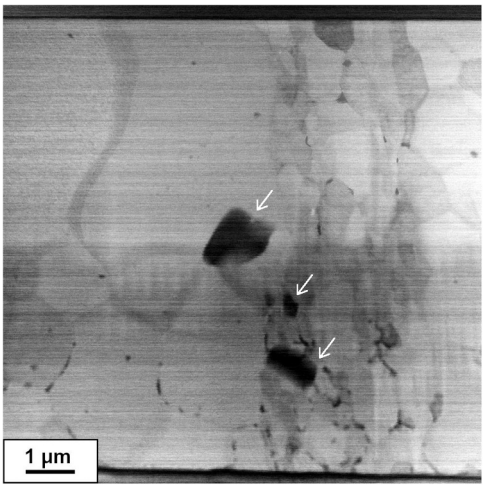

Fig. 12. HAADF image of Al99.5 with 0.5 % of CNTs composite after HPT processing and annealing at 350ºC showing the distribution of individual CNTs (black in HAADF contrast) and their agglomerates (marked with arrows).

Table 3
Grain size and mechanical properties of Al-C nanocomposites composites [10,26,27,48].

Sample	Processing	Grain size [nm]	Hardness [Hv]	Ref.
Al 99.99 + 0.5 % CNTs and 1 %CNTs	• Direct mixing 50 turns	210 230	75 75	Present work
Al 99.5 + 0.5 % CNTs and 1 %CNTs	• Direct mixing 50 turns	235 190	95 105	Present work
Al 99.99 % powder + 5 wt % CNTs	• Plastic consolidation of powders • Followed by HPT at RT, 2.5 GPa, 30 turns	170	76	[26]
Al 1050 powder + 5 wt% CNTs modified with Cu	• Plastic consolidation of powders • Followed by HPT at 473 K, 6.0 GPa, 10 turns	100	150	[27]
Al 1050 powder + 1.5 and 2 wt % CNTs	• Consolidation of powders using HIP • Followed by HPT at RT, 5.0 GPa, 5 turns	150	100	[48]
Al1050 powder + 5 wt% GNPs	• Compaction of powders • Followed by HPT at 298 K, 373 K, and 473 K, 6.0 GPa, 1, 5, 10 and 20 turns	160	110	[10]
Al 99,99 % + 5mass% CNT	• Al powder + CNT mixted in ethanol under ultrasonic condition 5 min, then ethanol evaporated • Mixted powders 0,35 g put into HPT anvil, HPT processed 2,5 GPa 1 rpm, 30 T	100	76	[26]

[50,51] as given by the following relationship which is reformulated in terms of hardness to give

$$H = H_o + k_H d^{-1/2} \quad (1)$$

where H is the hardness, H_o and k_H are material constants and d is the average grain size.

To further check on the applicability of the Hall-Petch relationship for the aluminium nanocomposites fabricated by HPT processing, the microhardness values obtained at the edges of the disks were plotted in Fig. 14 as a function of $d^{-1/2}$ together with datum points obtained from the initial coarser-grained alloys and the initial alloys after 10 HPT revolutions. In addition, trend lines for the Hall-Petch relationship for pure materials are also included. It is apparent that there is a clear difference in the distributions of the experimental points between the Al99.99 and Al99.5 nanocomposites and the trend lines for pure metals. For Al99.99 nanocomposites, the results are significantly shifted, even after 10 revolutions, from the linear relationship and this shift is the greater the higher the numbers of HPT revolutions. The hardness results for the samples after 20 and 50 revolutions are close to the trend line obtained for pure Al99.5. In addition, for Al99.5 matrix nanocomposites the results for 10 and 20 revolutions are close to the linear relationship for the pure alloy and there is a shift from the linear relationship only in the sample after 50 revolutions. It is important to note also that the data in Fig. 14 do not display the abrupt changes in slope that have been reported for several materials including Al alloys processed by HPT [52].

It is evident from these results that the key factor determining the strength of these nanocomposites is the good dispersion of nanofillers within the matrix. In the Al99.99 matrix nanocomposites, where the CNTs were uniformly distributed in the matrix even after only 10 turns, the mechanical properties were influenced not only by the increased grain refinement level according to the Hall-Petch relationship [50,51] but also by the individual CNTs which made a large contribution to the final strength of the nanocomposites. By contrast, the structure of the Al99.5 nanocomposites was determined primarily by the large CNTs agglomerates which favoured the fragmentation of the structure but contributed little to the overall strength. As a result, the linear trend was maintained for the samples after 10 and 20 revolutions and it was only after 50 rotations that there was a clear shift from linearity due to the improved distribution of CNTs in the matrix.

4.3. Thermal stability

The uniform distribution of CNTs in the aluminium matrix had a major impact not only on the grain refinement and mechanical properties of these nanocomposites but also on their thermal stability. In practice, the Al99.99 matrix nanocomposites had smaller CNT agglomerates than the Al99.5 matrix. Thus, Table 2 shows the proportion of visible agglomerates in the sample surfaces and for the Al99.99 matrix nanocomposites these values are significantly smaller (1.2 % and 1.8 % for 0.5 % and 1 % CNTs) than for the Al99.5 matrix nanocomposites (3.4 % and 4.5 % for 0.5 % and 1 % CNTs). The larger size of the visible agglomerates, for the same amount of added nanotubes, is associated with the poorer distribution of nanotubes in the metal matrix, where this had a significant effect on the role of these particles in blocking the movement of dislocations and grain boundaries. Fine particles located at grain boundaries may apply a pinning pressure thereby impeding the mobility of grain boundaries and blocking grain growth in addition to the overall effect of these CNTs, where this is described as the Zener pinning effect [53]. At the same time, the presence of large CNT agglomerates in the Al99.5 matrix samples leaves some areas without any particles to impede grain growth so that, as a result, some grains are blocked from growing whereas others are not blocked. This contributes to the abnormal growth of grains not blocked by CNTs, as described by the theory of abnormal grain growth due to the contribution from second phase particles [54], and this leads to heterogeneous microstructures in the Al99.5 matrix nanocomposites after annealing at 300ºC and 250ºC for 0.5 % and 1 % CNT additions.

In conclusion, the addition of CNTs has a positive effect on limiting the growth of aluminium grains during annealing but only when the CNT particles do not form large and numerous agglomerates but are instead sufficiently well distributed within the aluminium matrix. In the present direct synthesis procedure, the distribution of these CNTs is related both to the ductility of the matrix material and to the extent of

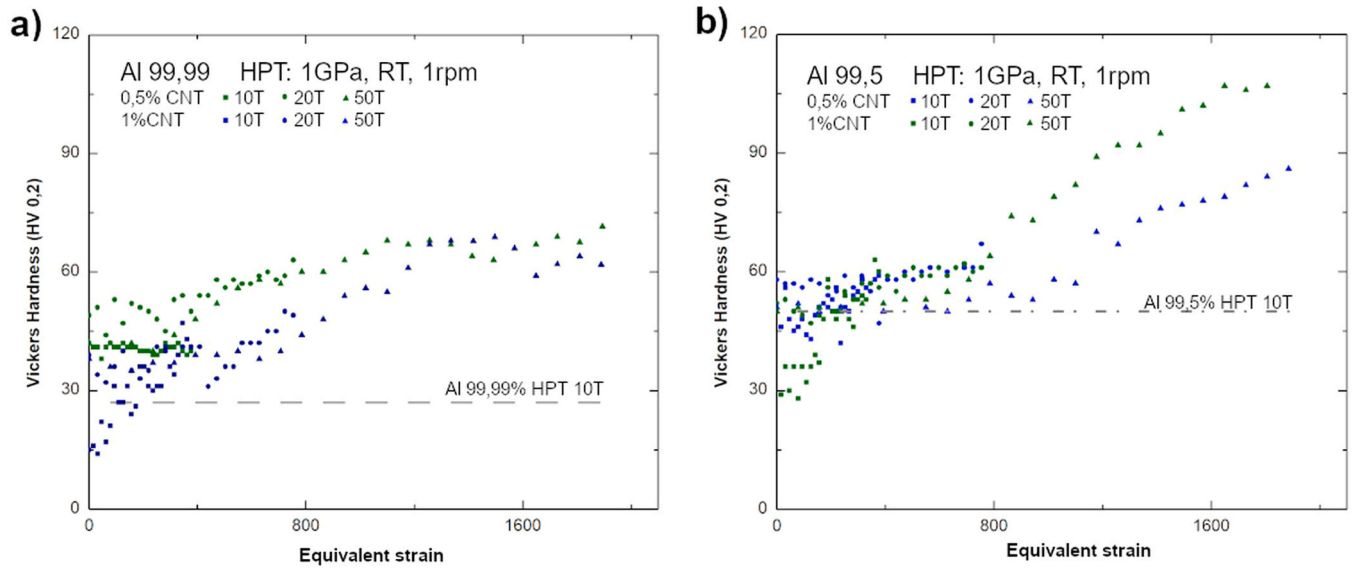

Fig. 13. Vickers microhardness plotted against equivalent strain for produced composites and reference literature data for Al 99.99 and Al 99.5 alloys.

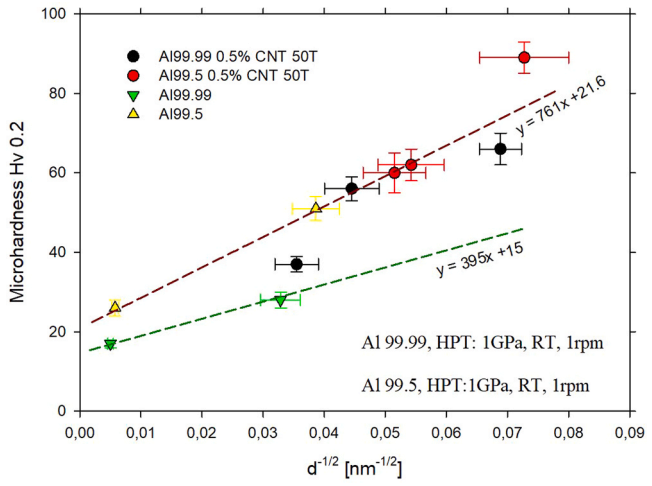

Fig. 14. Hall–Petch relationship for initial alloys in coarse-grained state and after processing through 10 HPT turns together with the data for Al-CNT composites fabricated in this work.

the applied deformation.

5. Summary and conclusions

- Al-CNTs nanocomposites were successfully produced by a direct synthesis procedure using HPT processing.
- A relatively good dispersion of CNTs was obtained within the Al matrix, especially for Al99.99.
- The addition of CNTs contributed to an increased grain size refinement by comparison with the matrix and this, together with the reinforcing effect of the CNTs, gave a significantly higher hardness of the nanocomposites compared to the matrix materials.
- For Al99.99 matrix nanocomposites, the hardness and microstructure remained stable even after annealing for 1 h at 400 °C. By contrast, the HPT-processed Al99.5 lost its UFG structure and enhanced mechanical properties after annealing at 150 °C. These results were associated with the good dispersion of CNTs in the Al99.99 matrix.
- For the Al99.5 matrix nanocomposites, the hardness was higher than for the pure metal for the total range of annealing temperatures. Nevertheless, there was noticeable grain growth accompanied by a decrease in hardness after annealing at 250 °C for the nanocomposite with 1 % CNTs and at 300 °C for the nanocomposite with 0.5 % CNTs and this was due to the poorer dispersion of CNTs and the increased number of large agglomerates.

CRediT authorship contribution statement

P. Bazarnik: Conceptualization, Methodology, Investigation, Data curation, Writing – original draft, Project administration, Funding acquisition. **M. Emerla:** Conceptualization, Methodology, Investigation, Validation, Writing – review & editing. **Y. Huang:** Processing, Investigation, data calculation. **M. Lewandowska:** Conceptualization, Writing – review & editing. **T.G. Langdon:** Conceptualization, Supervision, Writing – review & editing.

Declaration of Competing Interest

The authors declare that they have no known competing financial interests or personal relationships that could have appeared to influence the work reported in this paper.

Data availability

Data will be made available on request.

Acknowledgements

This work was carried out within an OPUS 19 project, Metal matrix composites fabricated by high-pressure torsion and reinforced with 2D and 3D nano-particles, funded by National Science Centre Poland under nb. 2020/37/B/ST5/01837. Two of the authors were supported by the European Research Council under ERC Grant Agreement No. 267464-SPDMETALS (YH and TGL).

References

[1] W. Zhang, J. Xu, Advanced lightweight materials for automobiles: a review, Mater. Des. 221 (2022), 110994, https://doi.org/10.1016/j.matdes.2022.110994.
[2] J. Hirsch, Recent development in aluminium for automotive applications, in: Trans. Nonferrous Met. Soc. China (English Ed., 24, 2014, pp. 1995–2002, https://doi.org/10.1016/S1003-6326(14)63305-7.
[3] V. Ferreira, P. Egizabal, V. Popov, M. García de Cortázar, A. Irazustabarrena, A. M. López-Sabirón, G. Ferreira, Lightweight automotive components based on

nanodiamond-reinforced aluminium alloy: a technical and environmental evaluation, Diam. Relat. Mater. 92 (2019) 174–186, https://doi.org/10.1016/j.diamond.2018.12.015.
[4] M.S. Sarfraz, H. Hong, S.S. Kim, Recent developments in the manufacturing technologies of composite components and their cost-effectiveness in the automotive industry: a review study, Compos. Struct. 266 (2021), 113864, https://doi.org/10.1016/j.compstruct.2021.113864.
[5] R.Z. Valiev, A.P. Zhilyaev, T.G. Langdon, Bulk Nanostructured Materials: Fundamentals and Applications, John Wiley & Sons, Inc, Hoboken, New Jersey, USA, 2014, https://doi.org/10.1142/9789814397988_0011.
[6] R.Z. Valiev, Y. Estrin, Z. Horita, T.G. Langdon, M.J. Zehetbauer, Y.T. Zhu, Fundamentals of superior properties in bulk NanoSPD materials, Mater. Res. Lett. 4 (2016) 1–21, https://doi.org/10.1080/21663831.2015.1060543.
[7] A.P. Zhilyaev, T.G. Langdon, Using high-pressure torsion for metal processing: fundamentals and applications, Prog. Mater. Sci. 53 (2008) 893–979, https://doi.org/10.1016/j.pmatsci.2008.03.002.
[8] P. Bazarnik, Y. Huang, M. Lewandowska, T.G. Langdon, Enhanced grain refinement and microhardness by hybrid processing using hydrostatic extrusion and high-pressure torsion, Mater. Sci. Eng. A 712 (2018) 513–520, https://doi.org/10.1016/j.msea.2017.12.007.
[9] M.I.A. El Aal, H.S. Kim, Wear properties of high pressure torsion processed ultrafine grained Al-7%Si alloy, Mater. Des. 53 (2014) 373–382, https://doi.org/10.1016/j.matdes.2013.07.045.
[10] Y. Huang, P. Bazarnik, D. Wan, D. Luo, P.H.R. Pereira, M. Lewandowska, J. Yao, B. E. Hayden, T.G. Langdon, The fabrication of graphene-reinforced Al-based nanocomposites using high-pressure torsion, Acta Mater. 164 (2019) 499–511, https://doi.org/10.1016/j.actamat.2018.10.060.
[11] P. Bazarnik, Y. Huang, M. Lewandowska, T.G. Langdon, Structural impact on the Hall-Petch relationship in an Al-5Mg alloy processed by high-pressure torsion, Mater. Sci. Eng. A. 626 (2015) 9–15, https://doi.org/10.1016/j.msea.2014.12.027.
[12] M. Kawasaki, H.J. Lee, B. Ahn, A.P. Zhilyaev, T.G. Langdon, Evolution of hardness in ultrafine-grained metals processed by high-pressure torsion, J. Mater. Res. Technol. 3 (2014) 311–318, https://doi.org/10.1016/j.jmrt.2014.06.002.
[13] P. Král, J. Staněk, L. Kunčická, F. Seitl, L. Petrich, V. Schmidt, V. Beneš, V. Sklenička, Microstructure changes in HPT-processed copper occurring at room temperature, Mater. Charact. 151 (2019) 602–611, https://doi.org/10.1016/j.matchar.2019.03.046.
[14] V.V. Popov, E.N. Popova, A.V. Stolbovskiy, Nanostructuring Nb by various techniques of severe plastic deformation, Mater. Sci. Eng. A 539 (2012) 22–29, https://doi.org/10.1016/j.msea.2011.12.082.
[15] S. Sabbaghianrad, J. Wongsa-Ngam, M. Kawasaki, T.G. Langdon, An examination of the saturation microstructures achieved in ultrafine-grained metals processed by high-pressure torsion, J. Mater. Res. Technol. 3 (2014) 319–326, https://doi.org/10.1016/j.jmrt.2014.10.002.
[16] S. Sabbaghianrad, T.G. Langdon, Microstructural saturation, hardness stability and superplasticity in ultrafine-grained metals processed by a combination of severe plastic deformation techniques, Lett. Mater. 5 (2015) 335–340, https://doi.org/10.22226/2410-3535-2015-3-335-340.
[17] S. Sabbaghianrad, T.G. Langdon, An evaluation of the saturation hardness in an ultrafine-grained aluminum 7075 alloy processed using different techniques, J. Mater. Sci. 50 (2015) 4357–4365, https://doi.org/10.1007/s10853-015-8989-x.
[18] Y. Ito, K. Edalati, Z. Horita, High-pressure torsion of aluminum with ultrahigh purity (99.9999%) and occurrence of inverse Hall-Petch relationship, Mater. Sci. Eng. A. 679 (2017) 428–434, https://doi.org/10.1016/j.msea.2016.10.066.
[19] K. Edalati, Z. Horita, Significance of homologous temperature in softening behavior and grain size of pure metals processed by high-pressure torsion, Mater. Sci. Eng. A 528 (2011) 7514–7523, https://doi.org/10.1016/j.msea.2011.06.080.
[20] R.K. Islamgaliev, F. Chmelik, R. Kuzel, Thermal structure changes in copper and nickel processed by severe plastic deformation, Mater. Sci. Eng. A 234–236 (1997) 335–338, https://doi.org/10.1016/s0921-5093(97)00247-5.
[21] E. Schafler, R. Pippan, Effect of thermal treatment on microstructure in high pressure torsion (HPT) deformed nickel, Mater. Sci. Eng. A 387–389 (2004) 799–804, https://doi.org/10.1016/j.msea.2004.01.112.
[22] P. Bazarnik, M. Lewandowska, M. Andrzejczuk, K.J. Kurzydlowski, The strength and thermal stability of Al-5Mg alloys nano-engineered using methods of metal forming, Mater. Sci. Eng. A. 556 (2012) 134–139, https://doi.org/10.1016/j.msea.2012.06.068.
[23] R.Z. Valiev, R.K. Islamgaliev, N.F. Kuzmina, Y. Li, T.G. Langdon, Strengthening and grain refinement in an Al-6061 metal matrix composite through intense plastic straining, Scr. Mater. 40 (1999) 117–122, https://doi.org/10.1016/S1359-6462(98)00398-4.
[24] I. Sabirov, O. Kolednik, R. Pippan, Homogenization of metal matrix composites by high-pressure torsion, Metall. Mater. Trans. A Phys. Metall. Mater. Sci. 36 (2005) 2861–2870, https://doi.org/10.1007/s11661-005-0281-2.
[25] Y. Xue, B. Jiang, L. Bourgeois, P. Dai, M. Mitome, C. Zhang, M. Yamaguchi, A. Matveev, C. Tang, Y. Bando, K. Tsuchiya, D. Golberg, Aluminum matrix composites reinforced with multi-walled boron nitride nanotubes fabricated by a high-pressure torsion technique, Mater. Des. 88 (2015) 451–460, https://doi.org/10.1016/j.matdes.2015.08.162.
[26] T. Tokunaga, K. Kaneko, Z. Horita, Production of aluminum-matrix carbon nanotube composite using high pressure torsion, Mater. Sci. Eng. A 490 (2008) 300–304, https://doi.org/10.1016/j.msea.2008.02.022.
[27] S.H. Joo, S.C. Yoon, C.S. Lee, D.H. Nam, S.H. Hong, H.S. Kim, Microstructure and tensile behavior of Al and Al-matrix carbon nanotube composites processed by high pressure torsion of the powders, J. Mater. Sci. 45 (2010) 4652–4658, https://doi.org/10.1007/s10853-010-4382-y.
[28] D.D. Phuong, P. Van Trinh, N. Van An, N. Van Luan, P.N. Minh, R.K. Khisamov, K. S. Nazarov, L.R. Zubairov, R.R. Mulyukov, A.A. Nazarov, Effects of carbon nanotube content and annealing temperature on the hardness of CNT reinforced aluminum nanocomposites processed by the high pressure torsion technique, J. Alloy. Compd. 613 (2014) 68–73, https://doi.org/10.1016/j.jallcom.2014.05.219.
[29] S. Suárez, E. Ramos-Moore, B. Lechthaler, F. Mücklich, Grain growth analysis of multiwalled carbon nanotube-reinforced bulk Ni composites, Carbon 70 (2014) 173–178, https://doi.org/10.1016/j.carbon.2013.12.089.
[30] M. Darabi, M. Rajabi, B. Junipour, M.T. Noghani, The effect of sintering temperature on Cu-Cnts nano composites properties produced by pm method, Sci. Sinter. 50 (2018) 477–486, https://doi.org/10.2298/SOS1804477D.
[31] A.K. Shukla, N. Nayan, S.V.S.N. Murty, S.C. Sharma, P. Chandran, S.R. Bakshi, K. M. George, Processing of copper-carbon nanotube composites by vacuum hot pressing technique, Mater. Sci. Eng. A. 560 (2013) 365–371, https://doi.org/10.1016/j.msea.2012.09.080.
[32] M. Jafari, M.H. Abbasi, M.H. Enayati, F. Karimzadeh, Mechanical properties of nanostructured Al2024-MWCNT composite prepared by optimized mechanical milling and hot pressing methods, Adv. Powder Technol. 23 (2012) 205–210, https://doi.org/10.1016/j.apt.2011.02.008.
[33] C. Guiderdoni, C. Estournès, A. Peigney, A. Weibel, V. Turq, C. Laurent, The preparation of double-walled carbon nanotube/Cu composites by spark plasma sintering, and their hardness and friction properties, Carbon 49 (2011) 4535–4543, https://doi.org/10.1016/j.carbon.2011.06.063.
[34] H. Kurita, H. Kwon, M. Estili, A. Kawasaki, Multi-walled carbon nanotube-aluminum matrix composites prepared by combination of hetero-agglomeration method, spark plasma sintering and hot extrusion, Mater. Trans. 52 (2011) 1960–1965, https://doi.org/10.2320/matertrans.M2011146.
[35] G.F. Korznikova, K.S. Nazarov, R.K. Khisamov, S.N. Sergeev, R.U. Shayachmetov, G.R. Khalikova, J.A. Baimova, A.M. Glezer, R.R. Mulyukov, Intermetallic growth kinetics and microstructure evolution in Al-Cu-Al metal-matrix composite processed by high pressure torsion, Mater. Lett. 253 (2019) 412–415, https://doi.org/10.1016/j.matlet.2019.07.124.
[36] B. Ahn, A.P. Zhilyaev, H.J. Lee, M. Kawasaki, T.G. Langdon, Rapid synthesis of an extra hard metal matrix nanocomposite at ambient temperature, Mater. Sci. Eng. A 635 (2015) 109–117, https://doi.org/10.1016/j.msea.2015.03.042.
[37] J.K. Han, K.D. Liss, T.G. Langdon, M. Kawasaki, Synthesis of a bulk nanostructured metastable Al alloy with extreme supersaturation of Mg, Sci. Rep. 9 (2019) 1–7, https://doi.org/10.1038/s41598-019-53614-3.
[38] J. Lipecka, M. Andrzejczuk, M. Lewandowska, J. Janczak-Rusch, K. J. Kurzydłowski, Evaluation of thermal stability of ultrafine grained aluminium matrix composites reinforced with carbon nanotubes, Compos. Sci. Technol. 71 (2011) 1881–1885, https://doi.org/10.1016/j.compscitech.2011.09.001.
[39] Y. Liu, C. Lu, H. Wang, A.K. Tieu, B. Liu, Microstructure evolution, lattice rotation retardation and grain orientation fragmentation in commercial purity aluminium deformed by high pressure torsion, J. Mater. Res. Technol. 9 (2020) 6642–6654, https://doi.org/10.1016/j.jmrt.2020.04.056.
[40] Y. Iwahashi, Z. Horita, M. Nemoto, T.G. Langdon, The process of grain refinement in equal-channel angular pressing, Acta Met. 46 (1998) 3317–3331, https://doi.org/10.1007/978-3-319-35107-0_5.
[41] Z. Horita, T. Fujinami, M. Nemoto, T.G. Langdon, Equal-channel angular pressing of commercial aluminum alloys: grain refinement, thermal stability and tensile properties, Metall. Mater. Trans. A Phys. Metall. Mater. Sci. 31 (2000) 691–701, https://doi.org/10.1007/s11661-000-0011-8.
[42] N. Wang, Y. Wen, L.Q. Chen, Pinning force from multiple second-phase particles in grain growth, Comput. Mater. Sci. 93 (2014) 81–85, https://doi.org/10.1016/j.commatsci.2014.06.030.
[43] J.H. Driver, Stability of nanostructured metals and alloys, Scr. Mater. 51 (2004) 819–823, https://doi.org/10.1016/j.scriptamat.2004.05.014.
[44] Z. Li, J. Wang, H. Huang, Influences of grain/particle interfacial energies on second-phase particle pinning grain coarsening of polycrystalline, J. Alloy. Compd. 818 (2020), https://doi.org/10.1016/j.jallcom.2019.152848.
[45] R. Kulagin, Y. Beygelzimer, Y. Ivanisenko, A. Mazilkin, H. Hahn, Modelling of High Pressure Torsion using FEM, Procedia Eng. 207 (2017) 1445–1450, https://doi.org/10.1016/j.proeng.2017.10.911.
[46] R. Sundeev, A. Shalimova, S. Rogachev, O. Chernogorova, A. Glezer, A. Ovcharov, I. Karateev, N. Tabachkova, Structural aspects of the formation of multilayer composites from dissimilar materials upon high-pressure torsion, Materials 16 (2023), https://doi.org/10.3390/ma16103849.
[47] Y. Beygelzimer, Vortices and mixing in metals during severe plastic deformation, Mater. Sci. Forum 683 (2011) 213–224, https://doi.org/10.4028/www.scientific.net/MSF.683.213.
[48] X. Yang, T. Zou, C. Shi, E. Liu, C. He, N. Zhao, Effect of carbon nanotube (CNT) content on the properties of in-situ synthesis CNT reinforced Al composites, Mater. Sci. Eng. A 660 (2016) 11–18, https://doi.org/10.1016/j.msea.2016.02.062.
[49] A. Vorhauer, R. Pippan, On the homogeneity of deformation by high pressure torsion, Scr. Mater. 51 (2004) 921–925, https://doi.org/10.1016/j.scriptamat.2004.04.025.
[50] E.O. Hall, The deformation and ageing of mild steel III discussion of results, Proc. Phys. Soc. Sect. B 64 (1951) 747–753.
[51] N.J. Petch, The cleavage strength of polycrystals, J. Iron Steel Inst. 174 (1953) 25–28.

[52] S. Dangwal, K. Edalati, R.Z. Valiev, T.G. Langdon, Breaks in the Hall–Petch relationship after severe plastic deformation of magnesium, aluminum, copper, and iron, Crystals 13 (2023) 413, https://doi.org/10.3390/cryst13030413.

[53] P.A. Manohar, M. Ferry, T. Chandra, Five decades of the Zener equation, ISIJ Int. 38 (1998) 913–924, https://doi.org/10.2355/isijinternational.38.913.

[54] A.J. McEvily, Fail. Fatigue (1974), https://doi.org/10.1016/b978-0-08-025437-1.50014-0.